Journal of Hazardous Materials 512 (2026) 142352

Contents lists available at ScienceDirect

Journal of Hazardous Materials

journal homepage: www.elsevier.com/locate/jhazmat

Simultaneous real-time estimation of airborne bacterial and fungal concentrations for indoor bioaerosol exposure surveillance via adenosine triphosphate (ATP) bioluminescence

Hyun Sik Ko, Jaeho Oh, Jungho Hwang *

Department of Mechanical Engineering, Yonsei University, Seoul 03722, Republic of Korea

HIGHLIGHTS

- Field-deployable BADD integrates wet-cyclone sampling and dual optofluidics.
- Time-resolved ATP kinetics enables differential real-time tracking of bacteria/fungi.
- Airborne LODs of 83–169 CFU/m^3 support rapid on-site bioaerosol surveillance.
- Field tests captured transient indoor bioaerosol fluctuations with ~15 min correction.

GRAPHICAL ABSTRACT

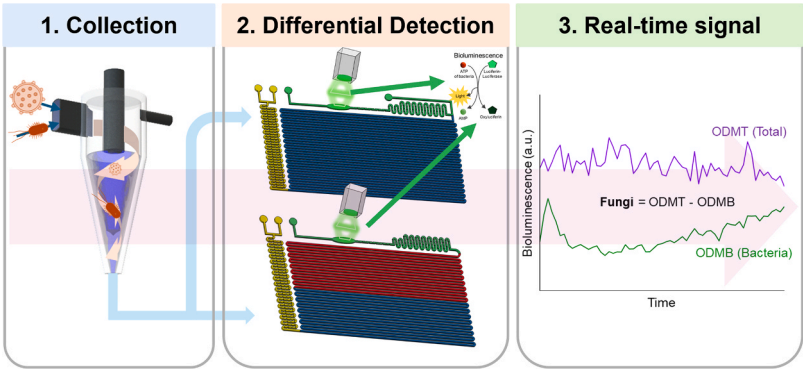

ARTICLE INFO

Keywords:
Real-time monitoring
Bioaerosol exposure
Indoor air
Hazard monitoring
ATP bioluminescence

ABSTRACT

Airborne bacteria and fungi are major components of indoor bioaerosol exposure and can contribute to adverse health outcomes, yet routine monitoring is often limited by the low time resolution and delayed results of culture-based methods. These limitations can obscure short-lived, potentially hazard-relevant fluctuations in indoor bioaerosol concentrations, reducing the utility of conventional methods for timely exposure screening and risk-informed environmental response. To address this gap, we developed a field-deployable, real-time monitoring system that combines wet-cyclone air sampling with dual optofluidic adenosine triphosphate (ATP) bioluminescence modules for differential estimation of airborne bacterial and fungal concentrations from a single collected sample. The system uses time-resolved lysis and bioluminescence responses to distinguish bacterial and fungal signals, enabling low-latency tracking of group-selective bioaerosol dynamics in indoor environments. We evaluated analytical performance through laboratory calibration and chamber tests and further demonstrated field applicability in occupied indoor spaces using comparisons with culture-based measurements and reference instruments. This system is intended as a complementary tool for bioaerosol exposure surveillance and risk screening, rather than a replacement for culture-based identification and confirmation workflows.

* Corresponding author.
E-mail address: hwangjh@yonsei.ac.kr (J. Hwang).

https://doi.org/10.1016/j.jhazmat.2026.142352
Received 23 February 2026; Received in revised form 25 April 2026; Accepted 8 May 2026
Available online 10 May 2026

1. Introduction

Bioaerosols are airborne particulate matter derived from biological sources, such as bacteria, fungi, and pollen [1]. The inhalation of bioaerosols can have various adverse health effects, including infections, allergic responses, toxic effects, and even cancer [2,3]. Globally, more than 250 million people are affected by bioaerosol-related diseases [4]. Although the risk of aerosol transmission is generally considered to be lower than that of direct person-to-person contact, the small size and lightweight of bioaerosols allow them to travel hundreds of meters, making transmission unpredictable and increasing exposure risks [5]. With increasing concerns regarding indoor and outdoor bioaerosol exposure, effective monitoring has become a public-health priority.

Adenosine triphosphate (ATP) bioluminescence has become a promising tool for rapid microbial quantification. This technique uses ATP as a universal indicator of metabolic activity, enabling luciferase to oxidize D-luciferin into oxyluciferin, emitting light proportional to the ATP content [6]. An ATP-based bioluminescence method requires correlation and calibration against culture-based measurements, as microbial air-quality guidelines are primarily defined based on the colony-forming units (CFU) per 1 m^3 air. The American Conference of Governmental Industrial Hygienists (ACGIH) recommends that indoor fungal concentrations remain below 1000 CFU/m^3 , while South Korea's Ministry of Environment stipulates separate standards for fungi (500 CFU/m^3) and bacteria (800 CFU/m^3) [7,8].

Several studies have adapted ATP-based bioluminescence methods for the detection of airborne bacteria. For example, Cho et al. (2020) used a wet cyclone for aerosol collection, followed by thermal lysis and ATP quantification [9]. Oh et al. (2023) applied a swab-filter-based impaction method with lysis buffer treatment [10]. Chen et al. (2024) extracted ATP from both bacteria and fungi to estimate total microbial activity and further employed loop-mediated isothermal amplification to identify specific pathogens [11]. More recently, Ko and Hwang (2026) reported a culture-independent fluorescence resonance energy transfer (FRET)-based biosensor for airborne bacterial monitoring using an ATP-specific aptamer, a fluorophore-labeled complementary DNA strand, and graphene oxide. By employing an indirect hybridization strategy to decouple fluorophore labeling from aptamer recognition, the FRET-based biosensor achieved femtomolar-level analytical sensitivity for ATP under indoor sampling conditions [12].

Despite these advances, previous studies have primarily focused on total microbial concentrations without distinguishing between bacteria and fungi. This represents a critical gap, as regulatory standards treat these organisms separately owing to their differing health implications and control requirements. To date, no existing method has enabled the simultaneous and differentiated quantification of airborne bacterial and fungal concentrations in real time.

Fig. 1 shows the concept of the time-resolved bioluminescence detection strategy. Because bacterial cells lyse more rapidly than fungal cells [13], bacteria release ATP earlier, whereas fungi release ATP later. Previous studies suggest that fungal cell disruption often requires more stringent or optimized mechanical and/or chemical treatment than bacterial cell disruption because fungal cell walls are generally more robust and compositionally complex [13–15]. Therefore, upon reagent injection, bacterial suspensions exhibit a sharp and immediate increase in bioluminescence, indicating rapid lysis and ATP release. Contrastingly, fungal suspensions exhibit a delayed and gradual rise in the signal, consistent with slower lysis kinetics. The observed time gap (Δt) confirms the feasibility of distinguishing bacterial and fungal ATP based on their different lysis dynamics. This time-resolved detection strategy enables the differential quantification of bacterial and fungal concentrations within a single analytical cycle, overcoming the limitations of conventional ATP-based methods that only report total ATP. For the selected experimental conditions (details are provided in Section 1 of Supplementary Material), this strategy was verified experimentally under static conditions.

To preliminarily validate this strategy, static experiments were performed using mixed bacterial and fungal suspensions (Fig. 2). Distinct temporal profiles were observed, with bacteria producing an immediate rise in signal, whereas fungi showed a delayed increase, confirming the time gap between their lysis kinetics (Fig. 2a). When a bacterial lysis buffer was applied, only bacterial ATP was released, enabling selective bacterial detection (Fig. 2b). In contrast, the use of a cell lysis buffer released ATP from both bacteria and fungi, yielding a total microbial signal (Fig. 2c). Taken together, these results establish the feasibility of differentiating bacterial and fungal ATP under static conditions. Building on this principle, we developed and evaluated an integrated Bio-Aerosol Detection Device (BADD) for field-deployable, real-time differential monitoring of airborne bacteria and fungi, aimed at low-latency indoor bioaerosol exposure surveillance.

2. BioAerosol Detection Device (BADD)

We designed a prototype BADD for the real-time and on-site quantification of airborne bacteria and fungi using time-resolved ATP bioluminescence (The prototype BADD was fabricated by ART Plus (Icheon, Republic of Korea)). The system consisted of a wet cyclone for bioaerosol sampling, as well as two optofluidic detection modules for sequential ATP measurement, both housed within a light-shielded chamber (Fig. 3a). Each detection module comprised a microfluidic chip, in which cell lysis and bioluminescent reactions occurred, and an optical sensor that detected emitted light. A single wet cyclone was intentionally used so that same hydrosol sample could be supplied to both detection modules. This shared-sample configuration reduced inter-sampler variability and supported synchronized comparison between the bacterial signal measured by the optofluidic detection module for bacteria (ODMB) and the total-microbial signal measured by the optofluidic detection module for total microorganism (ODMT).

2.1. Wet cyclone

The tangential inlet generated a helical airflow that formed a thin liquid film along the inner wall of the conical structure (Fig. 3b). Airborne particles entering the cyclone were impacted onto this film and became suspended in the liquid medium. The resulting hydrosol, which contained concentrated bioaerosols, was subsequently delivered to the detection modules. The wet cyclone design is described in Section 2 of Supplementary Material (Figure S2). Details regarding the collection

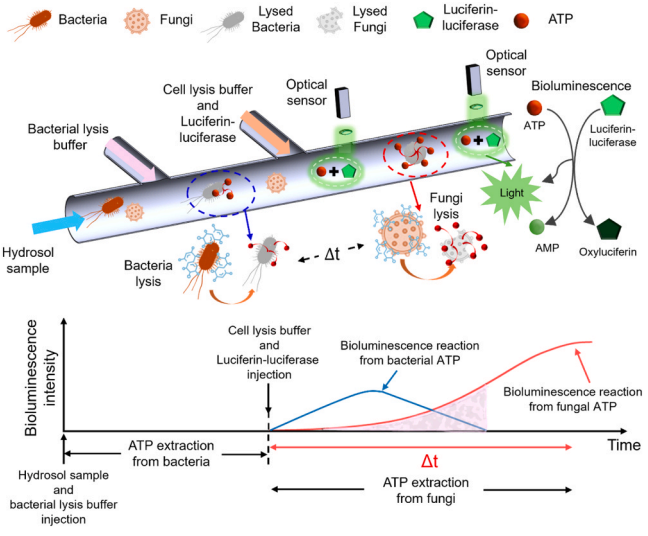

Fig. 1. Time-resolved optofluidic detection strategy for simultaneous quantification of adenosine triphosphate (ATP) bioluminescence signals originating from airborne bacteria and fungi.

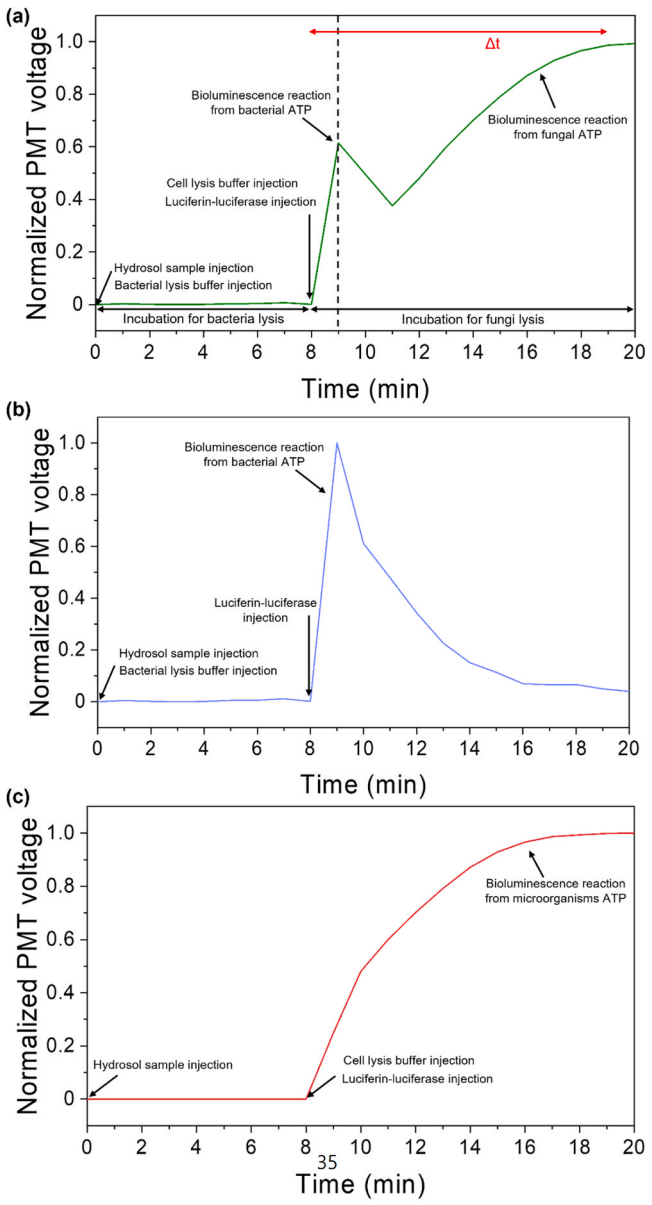

Fig. 2. Preliminary validation of time-resolved detection strategy under static conditions. (a) Time-resolved bioluminescence response of bacterial and fungal suspensions. (b) Selective bacterial detection performed using bacterial lysis buffer. (c) Total microbial detection performed using cell lysis buffer.

efficiency test are provided in Section 3 of Supplementary Material (Figure S3).

Airborne microorganisms exist at low concentrations (order of several hundred CFU/m^3), especially in indoor environments [16–18]. Meanwhile, ATP bioluminescence-based detection typically requires a minimum concentration of several hundred CFU/mL for reliable quantification [19,20]. Therefore, to bridge this gap, an enrichment factor of at least 10^5 is required, allowing for the conversion of low microbial loads from large volumes of air into small volumes of liquid suitable for sensitive analysis. The enrichment capacity (EC) can be calculated using the following equation:

$$EC = \frac{Q \times \eta_c}{L} \quad (1)$$

where Q is the air sampling flow rate (L/min), L is the liquid injection flow rate (L/min) and η_c is the collection efficiency.

The wet cyclone was connected to an air pump that drew ambient air

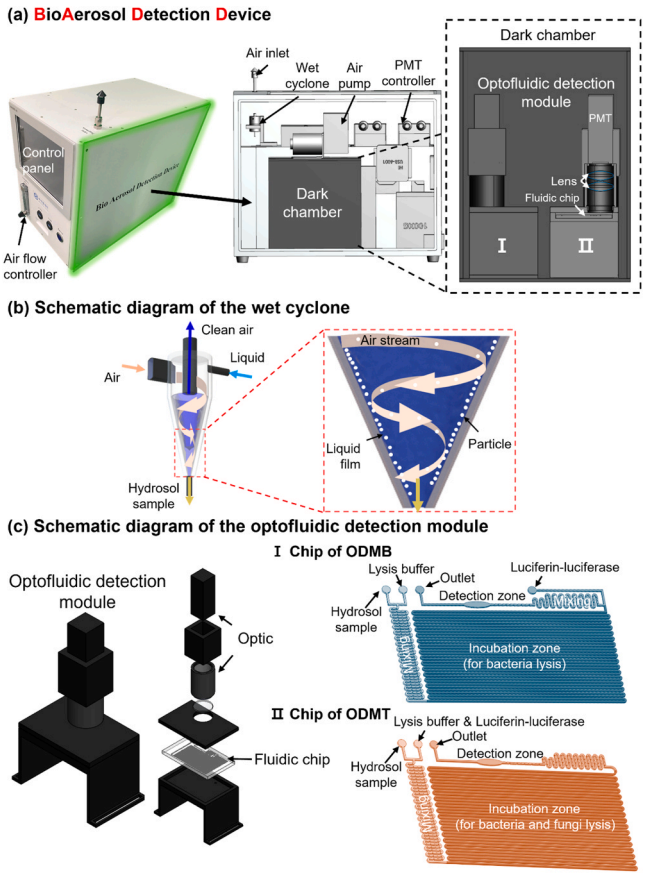

Fig. 3. (a) Components of BADD. (b) Working principle of wet cyclone. (c) Bioluminescence detection in optofluidic detection modules.

at a flow rate of approximately 15 L/min. To achieve an enrichment factor of at least 10^5, deionized water (DI water) was continuously injected into the cyclone at a rate of 150 μL/min during air sampling (η_c was assumed to be nearly unity). However, owing to evaporation occurring inside the cyclone, a portion of the injected liquid was lost. Empirically, this evaporative loss was estimated to be approximately 80 μL/min under the studied operating conditions. Details of the calculations are presented in Section 4 of Supplementary Material. As a result, the liquid flow rate available for downstream analysis was approximately 70 μL/min. This value was determined to be optimal for balancing the desired concentration factor and ensuring a sufficient volume for ATP extraction and detection. Under these conditions, the enrichment capacity was $EC \approx 2.14 \times 10^5$.

2.2. Optofluidic detection modules

To minimize the interference between bacterial and fungal ATP signals during bioluminescence measurements (see shaded region of the graph in Fig. 1), two optofluidic detection modules, each equipped with a dedicated microfluidic chip, were independently configured. Each module comprised a microfluidic chip connected to an optical sensing unit, peristaltic pumps for liquid handling, and reagent reservoirs.

2.2.1. Optofluidic detection module for bacteria

An ODMB was designed for the rapid detection of bacterial ATP. It operated with a bacterial lysis buffer (35 μL/min) and a luciferin–luciferase solution (70 μL/min). When a sample was introduced at 35 μL/min, bacterial cells were quickly lysed in the mixing zone (residence time of 30 s), releasing ATP. The combined stream (70 μL/min) then flowed through the incubation zone (8 min) to allow ATP

extraction, after which the released ATP immediately reacted with luciferase in the detection zone to generate a bioluminescent signal (Fig. 3c-I). The ODMB chip design is presented in detail Section 5 of Supplementary Material (Figure S5a).

2.2.2. Optofluidic detection module for total microorganism

Contrastingly, an ODMT introduced a time delay to ensure sufficient lysis of fungal cells, which generally lyse more slowly than bacteria. Following this delay, the system measured the total ATP signal originating from both bacteria and fungi (Fig. 3c-II). By subtracting the bacterial ATP signal (obtained from the ODMB) from the total ATP signal, the fungal ATP contribution could be isolated, allowing for an independent quantification of bacterial and fungal ATP. The ODMT chip design is presented in detail in Section 5 of Supplementary Material (Figure S5b). In this configuration, both the sample and the premixed reagent were introduced at 35 μL/min, yielding a total flow rate of 70 μL/min.

2.2.3. Mixing performance in the microfluidic chip

The microfluidic chips used in the ODMB and ODMT modules shared identical geometries in the mixing zone. Mixing performance was assessed using an image-based colorimetric method, in which the saturation component in the HSV (Hue, Saturation, Value) color space served as a quantitative indicator of color homogeneity [21,22]. In summary, optical images of the inlet and outlet regions were analyzed to calculate the mean and standard deviation of the saturation values, with reduced saturation heterogeneity indicating improved mixing. As detailed in Section 6 of Supplementary Material, the ODMB chip showed progressive improvements in mixing from the inlet to the outlet at each stage, confirming the effectiveness of its two-step mixing design.

2.2.4. Lysis performance in the microfluidic chip

The microfluidic chips used in the ODMB and ODMT modules shared identical geometries in the incubation zone. Lysis performance was evaluated by comparing the bioluminescence signals obtained at different lysis times (4, 8, and 12 min). The times were changed by adjusting the inlet flow rate. As described in Section 7 of Supplementary Material (Figure S7), the 4 min condition produced no detectable or weaker signals, whereas the 8 min and 12 min conditions showed overall comparable signal levels for the tested microorganisms. These results indicate that, under the flow and reagent conditions used in this study, a lysis time of approximately 8 min was sufficient to generate ATP-derived bioluminescence signals.

2.2.5. Bioluminescence detection

The optical detection zone of each module was designed as an elliptical area (approximately 8 mm × 2 mm) to enhance light collection efficiency. Two 1-in convex lenses (LB1761-A, Thorlabs Inc.) focused the emitted light onto a photomultiplier tube (PMT; H10723–110, Hamamatsu Photonics), which converted the optical signal into an electrical output. Further details on the optical configuration are provided in Section 8 of Supplementary Material.

3. Materials and methods

3.1. Preparation of test particles

Polystyrene latex particles with diameters of 80 nm, 350 nm, 500 nm, 1.0 μm, and 1.5 μm were purchased from Thermo Fisher Scientific (USA) and used to evaluate collection efficiency of the wet cyclone. The experimental methods and results used for evaluating the collection efficiency of the wet cyclone are thoroughly described in Section 3 of Supplementary Material.

The test microorganisms used were the Gram-positive bacterium *Staphylococcus aureus* (*S. aureus*; KCTC 1621), the representative Gram-negative bacterium *Escherichia coli* (*E. coli*; ATCC 25922), and the fungus *Candida albicans* (*C. albicans*; KCTC 77556). These strains were purchased from Korean Collection for Type Cultures (KCTC) and American Type Culture Collection (ATCC). These microorganisms are commonly found in indoor environments and have been evaluated in various bioaerosol studies [23–25].

3.1.1. Bacterial suspension preparation

The bacteria were incubated in tryptic soy broth (BD Difco, Sparks, MD, USA) at 37 °C under shaking (200 rpm) for 24 h. When the bacterial suspensions reached an optical density of 1.0 at 600 nm, the cells were harvested via centrifugation at 5000 ×g for 10 min and washed three times using DI water to remove the medium residues. The final concentrations of the cultured *S. aureus* and *E. coli* suspensions were both approximately 10^8 CFU/mL.

3.1.2. Fungal suspension preparation

The fungi were incubated in sabouraud dextrose broth (BD Difco, Sparks, MD, USA) at 37 °C under shaking (200 rpm) for 48 h. When the fungal suspension reached an optical density of 1.0 at 600 nm, the cells were collected via centrifugation at 5000 ×g for 10 min and washed thrice using DI water to remove residues. The concentration of resulting fungal suspension was approximately 10^7 CFU/mL.

3.2. Bioluminescent reagents

3.2.1. Reagents for ODMB

To identify the most effective lysis reagent for bacterial ATP detection, we evaluated several commercially available lysis buffers, including a Bacterial Protein Extraction Reagent (B-PER; Thermo Fisher Scientific, USA), cOmplete™ Lysis-M EDTA-free (Lysis-M; Roche, Switzerland), and Bacterial Cell Lysis Buffer (GoldBio, USA). Each lysis reagent was added to the bacterial suspension to disrupt the cell membrane and release intracellular ATP. The luciferin–luciferase reaction was performed using the ATP Bioluminescence Assay Kit CLS II (Roche, Basel, Switzerland), which provided the enzymatic components required for ATP-dependent luminescence. This configuration allowed for a fair comparison of lysis efficiency across different reagents by ensuring that the luminescence intensities reflected ATP release rather than reagent-specific assay chemistry.

A comparative analysis showed that B-PER produced the strongest and most consistent luminescence signals, indicating superior lysis efficiency for the bacterial samples. Therefore, B-PER was selected as the optimal lysis reagent for subsequent bacterial detection experiments. Detailed performance comparisons of the evaluated reagents are presented in Section 9 of Supplementary Material (Figure S9a).

3.2.2. Reagents for ODMT

To identify effective lysis reagents suitable for detecting a broad range (in terms of concentration) of fungi, comparative experiments were performed using several commercially available buffers. The reagents evaluated included a BacTiter-Glo™ Microbial Cell Viability Assay (BacTiter; Promega, USA), Cell Lysis Solution for Yeast and Fungi (CLS-Y; MP Biomedicals, USA) and Yeast Protein Extraction Reagent (Y-PER; Thermo Fisher Scientific, USA). BacTiter contains both a lysis buffer and a luciferin–luciferase enzyme system, allowing the direct induction of ATP-dependent bioluminescence upon cell lysis. In contrast, CLS-Y and Y-PER require an additional enzymatic step; the bioluminescence reaction was performed using the luciferin–luciferase reagent included in the ATP Bioluminescence Assay Kit CLS II (Roche, Basel, Switzerland).

Among the tested reagents, BacTiter demonstrated the highest signal intensity and most stable performance with fungal cells. Therefore, BacTiter was selected as the optimal lysis reagent for ODMT-based fungal detection. Detailed comparative results are provided in Section 9 of Supplementary Material (Figure S9b).

3.3. Standard curves for ATP solution

Fig. 4a shows the experimental setup used to assess the detection capabilities for the ODMB and ODMT at various ATP concentrations. An ATP solution was prepared by dissolving a certain amount of ATP powder (contained in the ATP Bioluminescence Assay Kit CLS II). The solution was then diluted to obtain a series of solutions of different concentrations. Subsequently, each diluted ATP solution was injected into the microfluidic chip. In the ODMB, B-PER and BacTiter solution (containing both the lysis buffer and luciferin–luciferase components) were sequentially injected. For the ODMT, a single reagent (BacTiter) containing both lysis buffer and luciferin–luciferase was used.

The resulting bioluminescence signal was measured using a PMT in each optical detection module. Two standard curves were established by correlating the bioluminescence intensities measured by the ODMB and ODMT, respectively, with ATP concentration (C_{ATP}, nM); $\Delta V_{ODMB} = a \times C_{ATP}$ and $\Delta V_{ODMT} = b \times C_{ATP}$, where a and b are proportionality constants. ΔV_{ODMB} and ΔV_{ODMT} denote output voltages (mV) from the PMTs of the ODMB and ODMT, respectively, relative to their baseline dark noises.

3.4. Standard curves for bacteria and fungi samples

The prepared bacterial and fungal suspensions were independently diluted. Thereafter, the diluted bacterial samples were injected into the ODMB. The B-PER and BacTiter solutions were then sequentially introduced according to a standard ATP test procedure. B-PER lysed bacterial cells, while BacTiter triggered an ATP-dependent bioluminescence reaction. The experiments were repeated using a diluted fungal sample injected into the ODMB. The experiments were also repeated by varying the concentrations of the bacterial and fungal samples (Fig. 4b-I). All luminescence signals from both the bacterial and fungal samples were recorded using a PMT integrated into the ODMB. Because ODMB lacks fungal lysis capability, the fungal samples generated only background-level luminescence.

The diluted bacterial samples were injected into the ODMT, after which a BacTiter solution was introduced into the ODMT. Since the BacTiter contained both a lysis component and a luciferin–luciferase enzyme, the resulting luminescence signal was recorded using a PMT integrated into the ODMT. The experiments were repeated using diluted fungal samples injected into the ODMT. In addition, the experiments were repeated by varying the concentrations of the bacterial and fungal samples (Fig. 4b-I).

For CFU analysis, each diluted sample (0.1 mL) was plated onto a growth medium. Tryptic soy agar (TSA) was used for bacterial cultures (incubated at 37 °C for 24 h), and Sabouraud dextrose agar (SDA) was used for fungal cultures (incubated at 37 °C for 48 h). Colony counts were recorded after incubation (Fig. 4b-II).

A standard curve for bacterial concentration was established by correlating the bioluminescence intensities measured from the ODMB with CFU values obtained from plate counting: $\Delta V_{ODMB} = c \times C_{bateria}$, $\Delta V_{ODMB} = \tilde{c} \times C_{fungi}$, where $C_{bateria}$ and C_{fungi} represent the bacterial and fungal concentrations (CFU/mL), and c and $\tilde{c}$ are proportionality constants. Notably, the proportionality constant $\tilde{c}$ was effectively zero because an ODMB cannot lyse fungal cells and, therefore, produces negligible luminescence for fungi. Similarly, the bioluminescence signals measured from the ODMT were correlated with CFU values to establish standard curves for both bacteria and fungi, following the relations $\Delta V_{ODMT} = d \times C_{bacteria}$, and $\Delta V_{ODMT} = e \times C_{fungi}$, where d and e are proportionality constants.

The ODMB signal reflected ATP derived exclusively from bacterial cells, while the ODMT signal represented total ATP from both bacteria and fungi. Accordingly, the bioluminescence from bacteria could be estimated as follows:

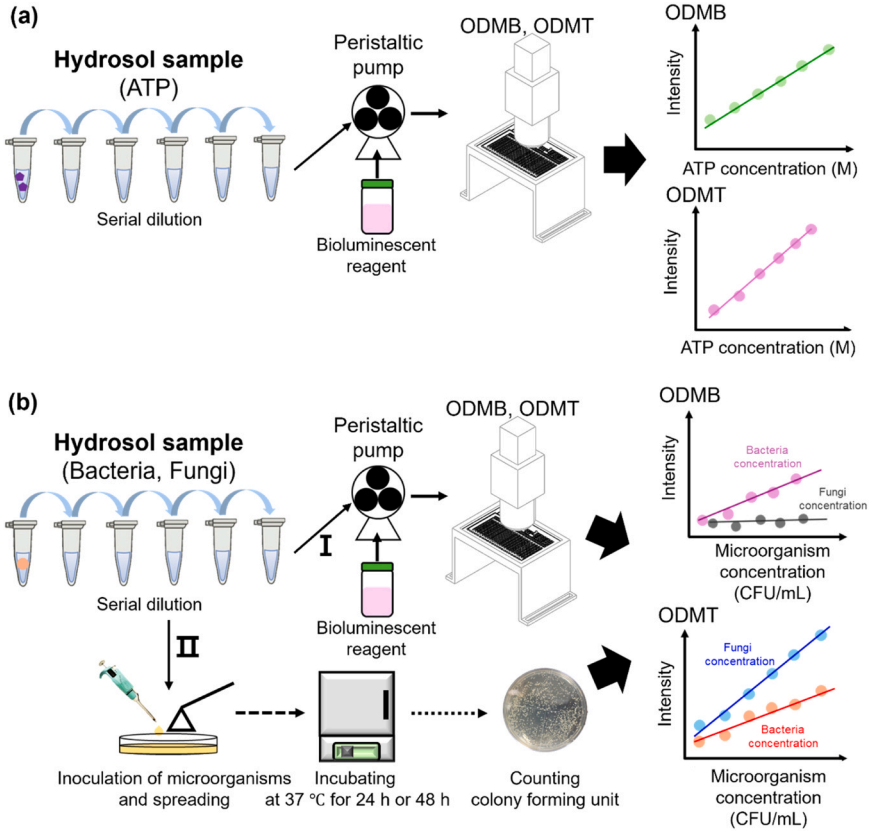

Fig. 4. (a) Schematic diagram of the process used to establish standard curves for ATP concentration by measuring bioluminescence signals in ODMB and ODMT. (b) Schematic of experimental setup for establishing calibration curves for bacteria and fungi.

$$C_{bacteria} = \frac{\Delta V_{ODMB}}{c} \quad (2)$$

Bioluminescence from fungi can be estimated by subtracting the ODMB signal from the ODMT signal, as follows (see Section 10 of Supplementary Material)

$$C_{fungi} = \frac{1}{e} \times \left(\Delta V_{ODMT} - \frac{d \times \Delta V_{ODMB}}{c} \right) \quad (3)$$

3.5. Chamber test of BADD for aerosolized bacteria and fungi

The performance of the BADD was evaluated under controlled laboratory conditions to assess its response to time-varying airborne microorganism concentrations. Fig. 5 shows a schematic diagram of the experimental setup used for this assessment.

S. aureus and *C. albicans* were used as representative bacterial and fungal species, respectively. For each test, 10 mL of bacterial suspension (~10^8 CFU/mL) or 10 mL of fungal suspension (~10^6 CFU/mL) was loaded into an Aerogen Pro nebulizer (Aerogen Ltd., Ireland) mounted on top of a sealed acrylic test chamber (500 × 500 × 500 mm^3, 125 L). The Aerogen Pro nebulizer used vibrating mesh technology to generate aerosols without requiring an external air supply. Each suspension was aerosolized for 10 min, and a small circulation fan was installed and operated during aerosolization to ensure uniform mixing of the bioaerosols within the chamber.

During aerosolization, the BADD recorded bioluminescence voltage signals at 1-min intervals to detect ATP-originated bioluminescence signals released from the collected airborne microorganisms. The BADD was operated at a sampling flow rate of 15 L/min. Simultaneously, an Aerodynamic Particle Sizer (APS; model 3321; TSI Inc., USA), which measured the particle size and concentration based on the aerodynamic diameter, was used to monitor the total particle concentration within the chamber over the same time intervals. Aerodynamic diameter is defined as the diameter of a spherical particle with a density of 1 g/cm^3 that settles at the same velocity as the particle in question under the influence of gravity. The APS was operated at a sampling flow rate of 1 L/min. Details regarding the APS are provided in Section 11 of Supplementary Material. To compensate for the total air flow rate of 16 L/min, make-up clean air was supplied to the acrylic chamber through a high efficiency particulate air filter. This setup ensured sufficient and stable airflow to support the operation of both the BADD and APS throughout the experiment.

The real-time bioluminescence signals recorded by the BADD were then compared with APS-derived particle concentration profiles to validate the responsiveness of the BADD to time-dependent microbial levels. Air sampling with MAS-100 NT was not performed because operating this sampler at 100 L/min for 1 min would withdraw a substantial fraction of the air from the chamber (125 L) within a short period, thereby significantly disturbing the chamber bioaerosol concentration profile. Meanwhile, the APS was operated at 1 L/min, resulting in a much smaller disturbance to the chamber atmosphere and making it more suitable for monitoring time-varying particle concentrations under controlled conditions. Therefore, APS measurements were used in the chamber test as a low-disturbance reference for time-varying aerosol concentrations. This chamber setup confirmed that the BADD could reliably detect and track dynamic changes in airborne bacterial and fungal concentrations in real time under controlled laboratory conditions.

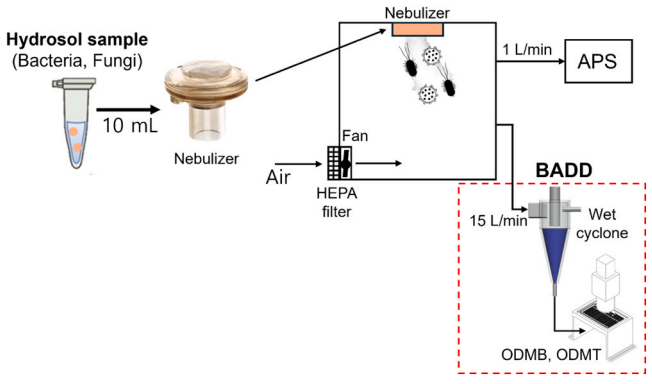

Fig. 5. Experimental chamber setup for evaluating airborne microbial detection using BADD system.

3.6. Field test of BADD

The measurement performance of the BADD was compared with that of the MAS-100 NT (Merck, Germany) through field tests conducted at two different locations within Yonsei University, Seoul, Korea: the lobby of the College of Engineering Building on August 16 (16:20–17:30) and the lobby of the Engineering Hall on September 24 (15:00–16:00), 2025. During the field measurements, the ambient temperature and relative humidity were 27.3 ± 0.6 °C and 58.6 ± 1.4%, respectively, in the lobby of the College of Engineering Building and 24.1 ± 0.4 °C and 68.2 ± 1.7%, respectively, in the lobby of the Engineering Hall.

The commercial air sampler (MAS-100 NT) complied with the ISO 14698 guidelines and fully met the cut-off-diameter requirement. The cut-off diameter refers to the aerodynamic particle size at which the sampling efficiency of a device drops to 50%, meaning that particles larger than this threshold are efficiently collected, whereas smaller particles may pass through or be collected with lower efficiency. Airborne microorganisms passed through 400 holes (each approximately 0.7 mm in diameter) and were directly collected on a TSA plate and SDA plate, for bacteria and fungi, respectively. The MAS-100 NT was operated at a flow rate of 100 L/min for 1 min over 10-min intervals. Thereafter, the bacterial and fungal colony numbers on the agar plate were counted after incubation for 72 h at 37°C and 120 h at 30°C, respectively. The concentration of bacteria ($C_{Bacteria,air}$) or fungi ($C_{Fungi,air}$) in air was calculated as follows [26]:

$$C_{bacteria,air} \text{ or } C_{fungi,air} = \frac{CFU_{bacteria} \text{ or } CFU_{fungi}}{V} \times 10[\mathrm{CFU/m^3}] \quad (4)$$

where $CFU_{bacteria}$ and CFU_{fungi} represent the colony counts of bacteria and fungi, respectively. V is the volume of the sampled air (L). Because 100 L of air was sampled using the MAS-100 NT, a correction factor of 10 was applied to express the results as CFU per cubic meter of air.

Based on the calibration functions in Eqs. (1), (2), and (3), the following inverse relationships were derived to convert the bioluminescence signals from the BADD into airborne microbial concentrations:

$$C_{bacteria,air} = \frac{\Delta V_{ODMB}}{c \times EC} \quad (5)$$

$$C_{fungi,\ air} = \frac{1}{e \times EC} \times \left(\Delta V_{ODMT} - \frac{d \times \Delta V_{ODMB}}{c} \right) \quad (6)$$

Airborne microbial concentrations were calculated from the MAS-100 NT data and compared to the BADD data. In parallel, the concentrations of airborne particles were continuously monitored using an APS.

4. Results and discussion

4.1. Standard curve results for ATP solution

To evaluate the performance of the optofluidic detection modules, the bioluminescence signals from ATP standards were measured across a range of concentrations.

Fig. 6a shows the relationship between ATP concentration and PMT voltage in the ODMB. The ODMB exhibited a linear response to ATP concentration (V_{ODMB} (mV) = 2.4 × 10^{-3} × C_{ATP} + 0.69), with a

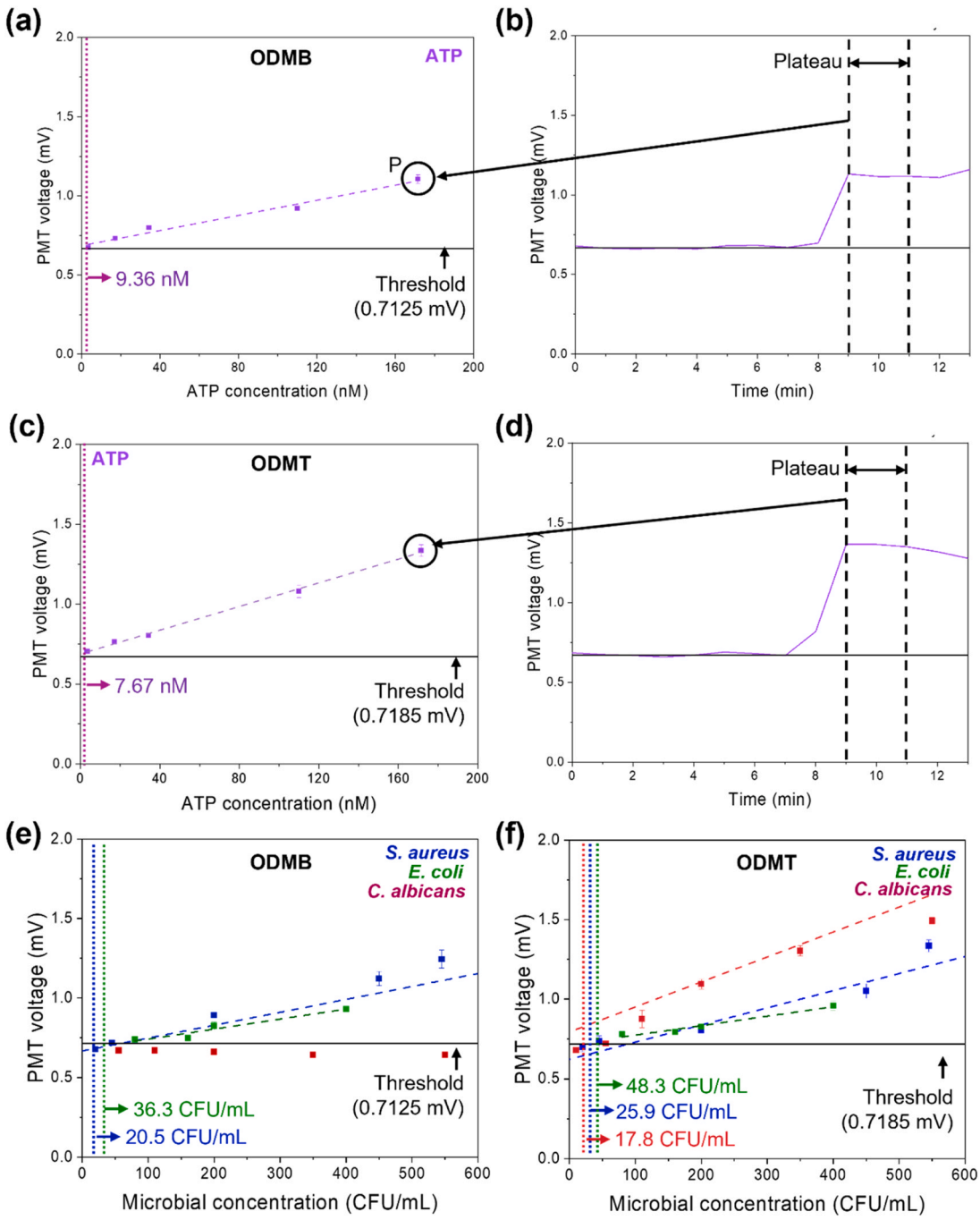

Fig. 6. Bioluminescence response of optofluidic detection modules. (a) Calibration curve of bacterial detection module (ODMB) as a function of ATP concentration ($R^2 = 0.98$). (b) Representative time-response curve of ODMB at an ATP concentration of 171.5 nM (datum point P in panel (a)). (c) Calibration curve of total microorganism detection module (ODMT) as a function of ATP concentration ($R^2 = 0.99$). (d) Representative time-response curve of ODMT at an ATP concentration of 171.5 nM. (e) Bioluminescence responses of ODMB to bacterial and fungal suspensions ($R^2 = 0.99$ for *S. aureus*, $R^2 = 0.93$ for *E. coli*). (f) Bioluminescence responses of ODMT to bacterial and fungal suspensions ($R^2 = 0.88$ for *S. aureus*, $R^2 = 0.96$ for *E. coli*, $R^2 = 0.96$ for *C. albicans*).

correlation coefficient of $R^2 = 0.98$. In ATP-free blanks acquired under identical optical settings, the baseline mean value (V_{blank}) was 0.69 mV while the standard deviation (σ_{blank}) was 0.0075 mV, resulting in a detection threshold of 0.7125 mV (According to Currie (1968) [27], the detection threshold is calculated as $V_{th} = V_{blank} + 3\sigma_{blank}$). By substituting 0.7125 mV into the linear response equation, C_{ATP} becomes 9.36 nM. (limit of detection [LOD]). Each data point shown in Fig. 6a was obtained by averaging the signal over 1-min intervals within the plateau region of the time-response curve. For example, Fig. 6b shows the time-response curve of the datum point 'P' of Fig. 6a, showing an increase in bioluminescence intensity and then a plateau at an ATP concentration of 171.5 nM.

Fig. 6c shows the relationship between ATP concentration and PMT voltage in the ODMT, which exhibited a linear response to ATP concentration ($V_{ODMT} = 3.7 \times 10^{-3} \times C_{ATP} + 0.69$; mV), with a correlation coefficient of $R^2 = 0.99$. In ATP-free blanks obtained under identical optical settings, the baseline mean and standard deviation for the ODMT was 0.690 ± 0.0095 mV, resulting in a detection threshold of 0.7185 mV. From this, the ATP LOD was determined to be 7.70 nM. Each data point shown in Fig. 6c was obtained by averaging the signal

over 1-min intervals within the plateau region of the time-response curve. Fig. 6d presents the time-response curve of the ODMT at an ATP concentration of 171.5 nM, showing an increase and then stabilization of the bioluminescence signal.

4.2. Standard curve results for bacterial and fungal solutions

To evaluate the performance of the optofluidic detection modules, the bioluminescence signals from microbial samples were also measured across a range of concentrations.

Fig. 6e shows the detection performance of the ODMB for bacteria and fungi at different concentrations. B-PER effectively lysed *S. aureus* and *E. coli*, allowing efficient ATP extraction and subsequent detection of bioluminescence signals with correlation coefficients of $R^2 = 0.99$ and $R^2 = 0.93$, respectively. Contrastingly, B-PER was ineffective against *C. albicans*, resulting in a negligible bioluminescence response, demonstrating that B-PER is suitable for selectively targeting bacterial cells. Based on these results, the ODMB output voltage exhibited a linear correlation with bacterial concentration ($V_{ODMB} = 1.1 \times 10^{-3} \times C_{bacteria\_positive} + 0.66$ for Gram-positive bacteria; $V_{ODMB} = 6.2 \times 10^{-4} \times C_{bacteria\_negative} + 0.67$ for Gram-negative bacteria).

Accordingly, the bacteria concentration in the liquid samples was quantified as:

$$C_{bacteria\_positive}\ (CFU/mL) = \frac{V_{ODMB} - 0.66}{11 \times 10^{-4}} \tag{7}$$

$$C_{bacteria\_negative}\ (CFU/mL) = \frac{V_{ODMB} - 0.67}{6.2 \times 10^{-4}} \tag{8}$$

By substituting detection threshold of 0.7125 mV into Eq. (7) and Eq. (8), the LODs calculated were as 20.5 CFU/mL for *S. aureus* (Gram-positive) and 36.3 CFU/mL for *E. coli* (Gram-negative).

Under identical ODMB and B-PER conditions, *E. coli* exhibited a slope of 6.2×10^{-4}, while *S. aureus* showed 1.1×10^{-3}. The higher bioluminescence signal of *S. aureus* was due to the fact that the intrinsic ATP content of Gram-positive bacteria is higher than that of Gram-negative bacteria [28]. Therefore, it was demonstrated that B-PER was sufficiently effective in releasing ATP, although Gram-positive *S. aureus* is generally more resistant to lysis because of its thick peptidoglycan layer.

Fig. 6f shows the detection performance of the ODMT for bacteria and fungi at different concentrations. Unlike the ODMB, the ODMT utilized a single reagent (BacTiter) that integrated both the lysis buffer with luciferin–luciferase, thereby enabling concurrent cell lysis and bioluminescence generation within the microfluidic channel. Under the selected reagent and assay conditions, the tested bacterial samples generated earlier bioluminescence signals than the tested fungal cells, whereas the fungal signal appeared after a longer lysis period. As a result, the fungal signal was generated primarily within the detection zone. The ODMT exhibited linear responses to the concentrations of Gram-positive bacteria, Gram-negative bacteria, and fungi ($V_{ODMT} = 1.1 \times 10^{-3} \times C_{bacteria_{positive}} + 0.65$, $V_{ODMT} = 5.9 \times 10^{-4} \times C_{bacteria_{negative}} + 0.71$; $V_{ODMT} = 1.6 \times 10^{-3} \times C_{fungi} + 0.69$).

The total ATP amount was first determined from the ODMT voltage signal to isolate the fungal signal from a Gram-positive bacteria–fungi mixture sample. The bacterial ATP contribution was then subtracted using the bacterial concentration obtained from the ODMB, yielding the net fungal ATP signal. The fungal concentration in the Gram-positive bacteria–fungi mixture sample ($C_{fungi,PB}$) was then derived from the isolated fungal ATP signal, using the following equation:

$$C_{fungi,PB}\ (CFU/mL) = \frac{1}{1.6 \times 10^{-3}} \left(V_{ODMT} - 0.69 - \frac{11 \times 10^{-4} \times (V_{ODMB} - 0.66)}{11 \times 10^{-4}}\right) \tag{9}$$

Similarly, the fungal concentration in the Gram-negative bacteria–fungi mixture sample ($C_{fungi,NB}$) was derived from the isolated fungal ATP signal, using the following equation:

$$C_{fungi,NB}\ (CFU/mL) = \frac{1}{1.6 \times 10^{-3}} \left(V_{ODMT} - 0.71 - \frac{5.9 \times 10^{-4} \times (V_{ODMB} - 0.67)}{6.2 \times 10^{-4}}\right) \tag{10}$$

Using ATP-free blanks measured in triplicates under identical optical settings, the detection threshold was defined as $V_{th} = V_{blank} + 3\sigma_{blank}$, where $\sigma_{blank}$is equal to0.0075 mV. By substituting $3\sigma_{blank}$ into the ODMT calibration curves, the ODMT LODs under single-analyte conditions were calculated as 25.9 CFU/mL for *S. aureus* (Gram-positive), 48.3 CFU/mL for *E. coli* (Gram-negative), and 17.8 CFU/mL for *C. albicans*, based on the respective calibration slopes of 1.1×10^{-3}, 5.9×10^{-4}, and 1.6×10^{-3}.

4.3. Chamber test results for aerosolized bacteria and fungi

Because bioaerosol concentrations can fluctuate abruptly, the rapid responsivity of the BADD was a critical indicator of its performance. To evaluate this capability, chamber experiments were conducted using aerosolized *S. aureus* and *C. albicans*.

For bacterial aerosols, the BADD voltage signals closely followed the sharp rise and fall of chamber concentrations, with an observed delay of approximately 15 min caused by sample transport through the wet cyclone and microfluidic modules. During aerosolization, the signals increased rapidly and then dropped sharply once nebulization was stopped, showing a strong correlation with the particle concentration dynamics (Fig. 7a).

For fungal aerosols, the BADD likewise exhibited a clear response to changes in *C. albicans* concentration. A delay of approximately 15 min was also observed, and the signals rose distinctly during aerosolization and decreased once the process ceased (Fig. 7b).

These results demonstrated that the BADD could rapidly respond to concentration changes in both bacteria and fungi. Notably, when comparing the BADD outputs with the actual concentration profiles, a temporal correction of approximately 15 min was required, confirming that the system could sensitively and reliably track abrupt variations in bioaerosol levels in real time.

4.4. Field test results of BADD

Two field tests were conducted at Yonsei University, Seoul, Korea: in the lobby of the College of Engineering Building on August 16 (16:20–17:30), and in the lobby of the Engineering Hall on September 24 (15:00–16:00), 2025.

During the first field test, the ODMB voltage signal closely followed the temporal variation in the total airborne particle number concentration recorded by the APS (Fig. 8a). Although the APS reported the total particle number concentration without distinguishing between biological components, the similar temporal patterns indicated that the ODMB reliably tracked fluctuations in bioaerosol loading through ATP-dependent detection. A 15-min temporal correction, consistent with the chamber results, was applied to align the ODMB signals with the APS and MAS-100 NT measurements.

Fig. 8b shows the airborne bacterial concentrations estimated from the ODMB voltage signals using Eqs. (1), (7), and (8). Eq. (1) provides the EC, while Eqs. (7) and (8) relate the ODMB voltage to bacterial concentration. Combining these relationships yields:

$$C_{bacteria\_positive,air}\ (CFU/m^3) = \frac{1}{EC} \times \frac{V_{ODMB} - 0.66}{11 \times 10^{-4}} \times 10^6 \tag{11}$$

$$C_{bacteria\_negative,air}\ (CFU/m^3) = \frac{1}{EC} \times \frac{V_{ODMB} - 0.67}{6.2 \times 10^{-4}} \times 10^6 \tag{12}$$

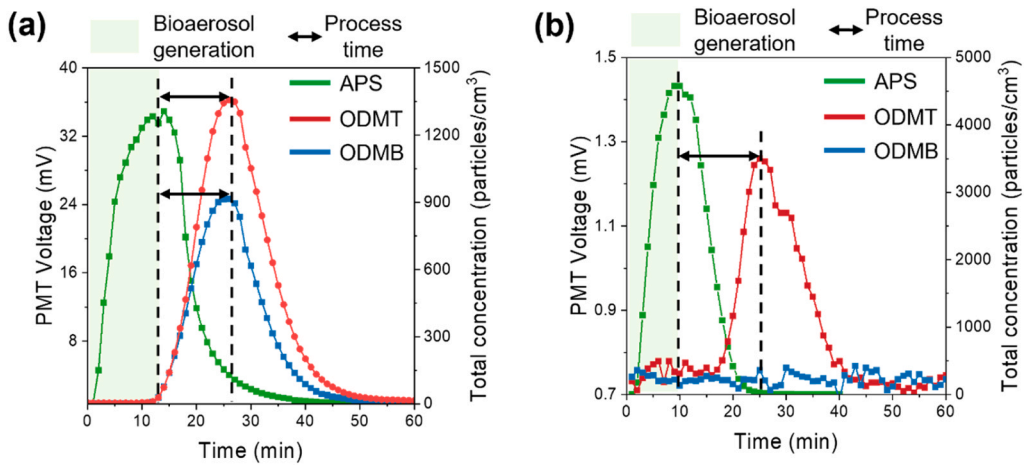

Fig. 7. (a) Bioluminescence intensity measured over time during exposure to aerosols generated by nebulizing bacterial suspension. (b) Bioluminescence intensity measured over time during exposure to aerosols generated by nebulizing fungal suspension. Chamber conditions: temperature = 26 ℃, relative humidity = 34%.

Because the conversion factors differed for Gram-positive and Gram-negative bacteria, the resulting absolute concentrations spanned a range; however, both estimates exhibited similar temporal trajectories, indicating that the ODMB robustly resolved time-varying bacterial loading under field conditions.

The ODMT exhibited a similar response, showing an initial increase followed by a decline that paralleled the APS trend (Fig. 8a). The airborne fungal concentrations estimated from the ODMT voltages using Eqs. (1), (9), and (10) are also shown in Fig. 8b. Eqs. (9) and (10) relate the ODMT voltage to the fungal concentration after subtracting the bacterial contribution measured using the ODMB. Here, fungi (PB) and fungi (NB) denote the fungal concentrations corrected by subtracting the Gram-positive- and Gram-negative-based bacterial contributions, respectively. Combining Eqs. (1), (9), and (10) yields:

$$C_{fungi(PB),air}\quad (CFU/m^3) = \frac{1}{EC}\times\frac{1}{1.6\times10^{-3}}(V_{ODMT}-0.69 - (V_{ODMB}-0.66))\times10^6 \tag{13}$$

$$C_{fungi(NB),air}\quad (CFU/m^3) = \frac{1}{EC}\times\frac{1}{1.6\times10^{-3}}(V_{ODMT}-0.71-0.95 \times (V_{ODMB}-0.67))\times10^6 \tag{14}$$

Under the present operating conditions (15-L/min wet cyclone), the airborne LODs were 96 CFU/m^3 (Gram-positive bacteria) and 169 CFU/m^3 (Gram-negative bacteria) for the ODMB, and 83 CFU/m^3 for the ODMT-derived fungi; thus, concentrations near these thresholds should be carefully interpreted.

In the second field test, both the ODMB and ODMT voltage signals (Fig. 8c) exhibited temporal variations that closely followed the APS trend, demonstrating consistent ATP-dependent detection of airborne bioaerosol fluctuations. The same 15-min temporal correction used at the first site was applied to align both modules with the APS measurements (and, where available, MAS-100 NT measurements). Fig. 8d shows the airborne bacterial concentrations estimated from the ODMB voltages using Eq. (11) and Eq. (12), as well as the airborne fungal concentrations estimated from the ODMT voltages using Eq. (13) and Eq. (14). The ODMB-derived bacterial concentrations and ODMT-derived fungal concentrations were comparable to the corresponding MAS-100 NT culture-based measurements in terms of magnitude and overall temporal tendency (Fig. 8d), while occasional deviations were expected owing to the differences between ATP-based and culture-based readouts. The dynamic indoor lobby environment (e.g., changes in occupancy, ventilation, and door-opening events) may have contributed to the observed rapid concentration excursions, emphasizing the value of real-time monitoring for capturing transient bioaerosol fluctuations.

4.5. Limitations of BADD in field applicability

When interpreting field measurements, differences between the ATP-based signals from the BADD and culture-based CFU counts can be attributed to four factors.

First, viable-but-nonculturable cells persist in a metabolically active state that retains intracellular ATP yet fails to produce colonies under routine plating; consequently, ATP levels can remain high while CFUs are low in the same air sample [29–31]. Second, cellular ATP content varies by taxon and physiological state; therefore, equal CFUs do not suggest equal ATP levels (and conversely, equal ATP levels do not suggest equal CFUs). For example, spores versus vegetative cells and exponential versus stationary phases exhibit order-of-magnitude differences in the number of ATPs per cell, leading to a systematic divergence between ATP- and CFU-based readouts as the community composition and growth state shift in the field [32]. Third, matrix constituents in real-world aerosols may affect luciferase kinetics and light yield, potentially biasing the bioluminescence response [33]. To evaluate this effect, potential interference from particulate matter during ATP-based detection was assessed (spike-and-recovery test). Resultantly, no significant interference was observed under the tested conditions. Detailed results are provided in Section 12 of Supplementary Material. Fourth, the composition and abundance of airborne microbial communities can vary substantially with location, season, and environmental conditions [34–36]. Accordingly, ATP–CFU calibration relationships established from laboratory-prepared single-species suspensions at controlled temperature and relative humidity (26 ℃, 34%) may not adequately account for the species-specific ATP content and lysis behavior of microorganisms present in real-world aerosols. In practical field applications, the laboratory-derived calibration coefficients may therefore be used as baseline values; however, when systematic deviations arise owing to site- or season-dependent shifts in airborne microbial communities, the application of additional correction factors based on verification against a reference culture-based method may be necessary to improve quantitative accuracy. Thus, reliable field quantification may be achieved through an initial site-specific verification followed by periodic validation, without necessitating re-establishment of the calibration relationship for every deployment.

From an operational perspective, field deployment is constrained by consumable usage and reagent storage stability. Under the present continuous-flow configuration, each reservoir in the BADD had an approximate capacity of 30 mL, corresponding to continuous operating durations of approximately 3.3 h for the DI-water supply, 14.3 h for the B-PER reservoir, and 4.8 h for the shared luciferin–luciferase reservoir.

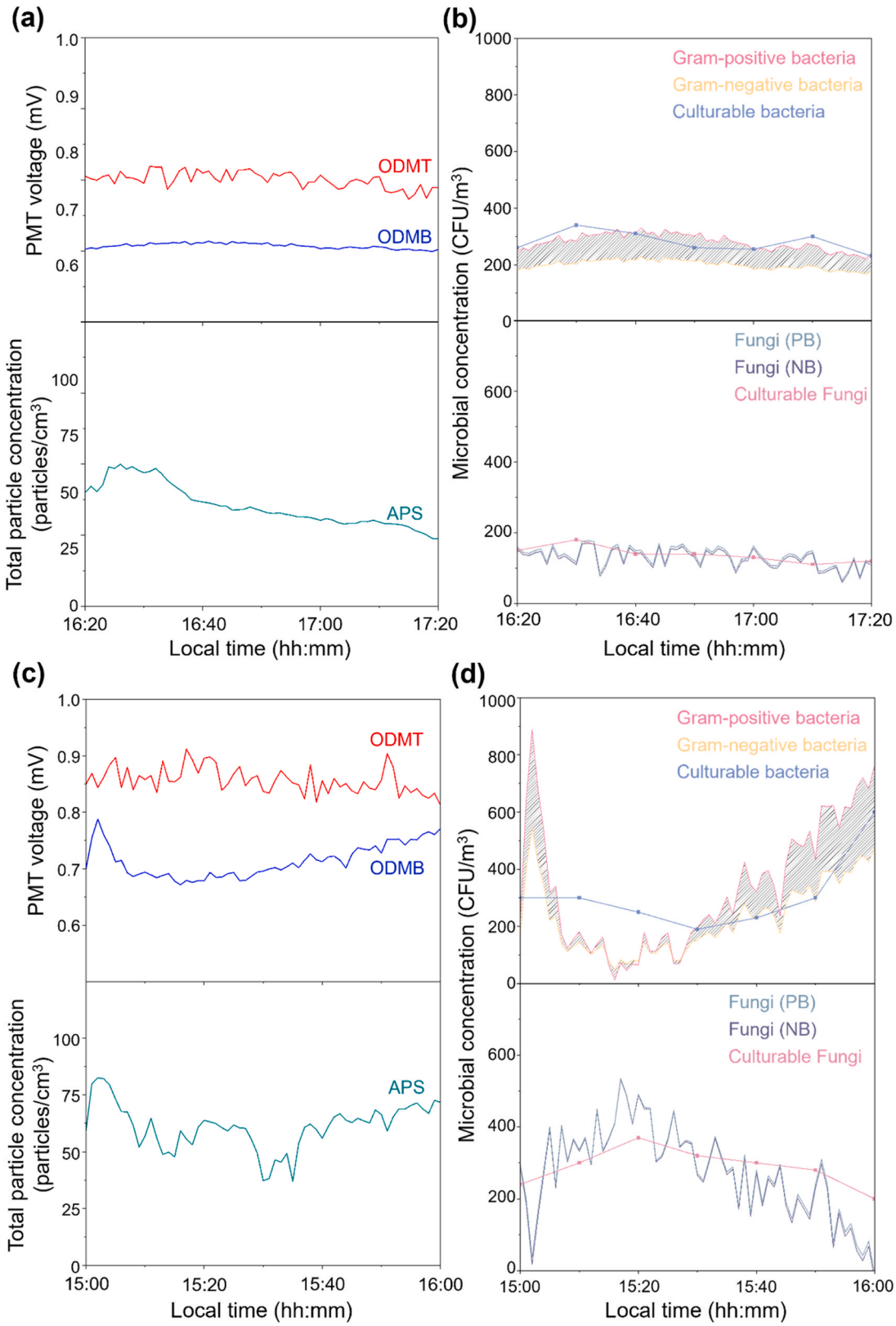

Fig. 8. Field test results of Bioaerosol Detection Device (BADD) conducted at two different locations within Yonsei University, Seoul, Korea. (a) Real-time voltage signals obtained from ODMB and ODMT modules compared with airborne particle concentration (APS) at the College of Engineering Building site. (b) Bacterial and fungal concentrations estimated from ODMB and ODMT voltages, compared with MAS-100 NT results. (c) Real-time ODMB, ODMT, and APS signals measured at the Engineering Hall site. (d) Bacterial and fungal concentrations estimated from ODMB and ODMT voltages, compared with MAS-100 NT results. Fungi (PB) represents fungal concentration estimated after accounting for contribution from Gram-positive bacteria, whereas Fungi (NB) represents fungal concentration estimated after accounting for contribution from Gram-negative bacteria. During the field measurements, the ambient temperature and relative humidity were 27.3 ± 0.6 °C and 58.6 ± 1.4%, respectively, at the College of Engineering Building site, and 24.1 ± 0.4 °C and 68.2 ± 1.7%, respectively, at the Engineering Hall site.

In addition, some assay reagents require controlled storage conditions to maintain stable performance over extended periods. Therefore, extended field deployment would benefit from cooled reagent compartments or replaceable reagent cartridges.

4.6. Complementary application of BADD and ultraviolet laser-induced fluorescence (UV-LIF) instruments

Ultraviolet laser-induced fluorescence (UV-LIF) instruments, such as ultraviolet aerodynamic particle sizer and wideband integrated bioaerosol sensor, are valuable tools for real-time bioaerosol monitoring because they provide rapid, single-particle fluorescence measurements. However, they generally report fluorescent particles rather than directly quantifying airborne bacterial and fungal concentrations in CFU-based terms, and their outputs may be influenced by non-biological fluorescent interferers [37]. In contrast, the ATP-based BADD quantifies metabolically active microbial burden after collection and lysis [38]. Moreover, the BADD is less dependent on intrinsic particle fluorescence and enables operational estimation of bacterial and fungal contributions through differential lysis. Accordingly, UV-LIF and ATP-based approaches should be regarded as complementary tools for bioaerosol surveillance.

5. Conclusion

This study developed a BADD that integrates a wet cyclone sampler (15 L/min) and dual optofluidic bioluminescence modules (ODMB and ODMT) for the real-time, simultaneous monitoring of airborne bacteria and fungi. The device enabled sequential ATP extraction and luminescence detection from bacteria and fungi, allowing the simultaneous quantification of both bacteria and fungi within a single analytical cycle. Laboratory validation demonstrated LODs of 20.5 CFU/mL for Gram-positive bacteria, 36.3 CFU/mL for Gram-negative bacteria, and 17.8 CFU/mL for fungi in liquid samples, corresponding to airborne limits of 96 CFU/m^3, 169 CFU/m^3, and 83 CFU/m^3, respectively. Furthermore, chamber tests confirmed a rapid response to time-varying concentrations with a temporal correction of approximately 15 min. Field tests conducted in two indoor environments (College of Engineering Building and Engineering Hall, Yonsei University) verified that the BADD outputs closely tracked the temporal variations in airborne bacterial and fungal concentrations measured using a commercial sampler (MAS-100 NT). Overall, the BADD provides a compact, field-validated system for low-latency monitoring of indoor bacterial and fungal bioaerosol fluctuations. Rather than replacing culture-based identification and confirmation workflows, it can serve as a complementary tool for bioaerosol exposure surveillance, risk screening, and risk-informed environmental response in dynamic indoor settings.

Environmental implications

Conventional culture-based bioaerosol monitoring often provides delayed results and may miss short-lived fluctuations relevant to indoor exposure and environmental response. The proposed BADD enables real-time, on-site differential tracking of airborne bacterial and fungal concentrations, supporting exposure surveillance and risk screening in dynamic indoor environments. As a complementary tool to culture-based identification workflows, this platform can improve the timeliness of bioaerosol monitoring and support risk-informed environmental management.

CRediT authorship contribution statement

Hyun Sik Ko: Writing – original draft, Visualization, Validation, Methodology, Investigation, Formal analysis, Data curation, Conceptualization. **Jaeho Oh:** Validation, Investigation, Formal analysis. **Jungho Hwang:** Writing – review & editing, Supervision, Funding acquisition, Conceptualization.

Declaration of Competing Interest

The authors declare that they have no known competing financial interests or personal relationships that could have appeared to influence the work reported in this paper

Acknowledgements

This research was supported by the National Research Foundation of Korea (NRF) grant funded by the Korea government (MSIT) (Grant No. RS-2025–00518644). This research was also supported by a grant from the Ministry of Health and Welfare, Republic of Korea, through the Korea Health Industry Development Institute's Korean-style ARPA-H Project (Grant No. RS-2025–25455741)

Appendix A. Supporting information

Supplementary data associated with this article can be found in the online version at doi:10.1016/j.jhazmat.2026.142352.

Data availability

Data will be made available on request.

References

[1] Hinds, W.C., Zhu, Y., 2022. Aerosol technology: properties, behavior, and measurement of airborne particles, third ed. John Wiley & Sons, New Jersey.
[2] Douwes, J., Thorne, P., Pearce, N., Heederik, D., 2003. Bioaerosol health effects and exposure assessment: progress and prospects. Ann Occup Hyg 47, 187–200. https://doi.org/10.1093/annhyg/meg032.
[3] Hilgenfeld, R., Peiris, M., 2013. From SARS to MERS: 10 years of research on highly pathogenic human coronaviruses. Antivir Res 100, 286–295. https://doi.org/10.1016/j.antiviral.2013.08.015.
[4] Cohen, A.J., Brauer, M., Burnett, R., Anderson, H.R., Frostad, J., Estep, K., et al., 2017. Estimates and 25-year trends of the global burden of disease attributable to ambient air pollution: an analysis of data from the Global Burden of Diseases Study 2015. Lancet 389 (10082), 1907–1918. https://doi.org/10.1016/S0140-6736(17)30505-6.
[5] Gormley, M., Marawska, L., Milton, D., 2020. It is time to address airborne transmission of coronavirus disease 2019 (COVID-19). Clin Infect Dis 71, 2311–2313. https://doi.org/10.1093/cid/ciaa939.
[6] Park, J.-W., Park, C.W., Lee, S.H., Hwang, J., 2015. Fast monitoring of indoor bioaerosol concentrations with ATP bioluminescence assay using an electrostatic rod-type sampler. PLoS One 10, e0125251. https://doi.org/10.1371/journal.pone.0125251.
[7] ACGIH, Guidelines for the assessment of bioaerosols in the indoor environment. American Conference of Governmental Industrial Hygienists (ACGIH), Cincinnati, Ohio, 1989.
[8] KME, 2021. Enforcement Rules of the Indoor Air Quality Control Act. (Written in Korean; Partial Revision in 2021). Korean Ministry of Environment (KME), Seoul, Republic of Korea.
[9] Cho, Y.S., Kim, H.R., Ko, H.S., Jeong, S.B., Kim, C.B., Jung, J.H., 2020. Continuous surveillance of bioaerosols on-site using an automated bioaerosol-monitoring system. ACS Sens 5, 395–403. https://doi.org/10.1021/acssensors.9b02001.
[10] Oh, J., Choi, J., Massoudifarid, M., Park, J.Y., Hwang, J., Lim, J., et al., 2023. Size-classified monitoring of ATP bioluminescence for rapid assessment of biological distribution in airborne particulates. Biosens Bioelectron 234, 115356. https://doi.org/10.1016/j.bios.2023.115356.
[11] Chen, Z., Liang, Z., Li, G., Das, R., Chen, P., An, T., 2024. Online monitoring system for qualitative and quantitative analysis of bioaerosols by combined ATP bioluminescence assay with loop-mediated isothermal amplification. Sci Total Environ 937, 173404. https://doi.org/10.1016/j.scitotenv.2024.173404.
[12] Ko, H.S., Hwang, J., 2026. Fluorescence Resonance Energy Transfer-Based Biosensor with Femtomolar Sensitivity for Culture-Independent Detection of Airborne Bacteria. Environ Sci Tech 60 (5), 4279–4288. https://doi.org/10.1021/acs.est.5c15957.
[13] Lomakina, G.Y., Modestova, Y.A., Ugarova, N., 2015. Bioluminescence assay for cell viability. Biochem (Mosc 80, 701–713. https://doi.org/10.1134/S0006297915060061.
[14] Klimek-Ochab, M., Brzezińska-Rodak, M., Żymańczyk-Duda, E., Lejczak, B., Kafarski, P., 2011. Comparative study of fungal cell disruption—scope and limitations of the methods. Folia Microbiol 56 (5), 469–475. https://doi.org/10.1007/s12223-011-0069-2.

[15] Rodríguez, A., Vaneechoutte, M., 2019. Comparison of the efficiency of different cell lysis methods and different commercial methods for RNA extraction from Candida albicans stored in RNAlater. Bmc Microbiol 19 (1), 94. https://doi.org/10.1186/s12866-019-1473-z.
[16] Karbowska-Berent, J., Górny, R.L., Strzelczyk, A.B., Wlazło, A., 2011. Airborne and dust borne microorganisms in selected Polish libraries and archives. Build Environ 46 (10), 1872–1879. https://doi.org/10.1016/j.buildenv.2011.03.007.
[17] Osaro, E.F., Ufuoma, I.O., Dorcas, A.O., 2008. Hospital indoor airborne microflora in private and government owned hospitals in Benin City, Nigeria. World J Med Sci 3 (1), 34–38.
[18] Jeong, S.B., Ko, H.S., Heo, K.J., Shin, J.H., Jung, J.H., 2022. Size distribution and concentration of indoor culturable bacterial and fungal bioaerosols. Atmos Environ X 15, 100182. https://doi.org/10.1016/j.aeaoa.2022.100182.
[19] Promega Corporation, BacTiter-Glo™ Microbial Cell Viability Assay: Technical Bulletin, ⟨https://www.promega.com/-/media/files/resources/protocols/technical-bulletins/101/bactiter-glo-microbial-cell-viability-assay-protocol.pdf⟩, 2019 (accessed 30 January 2026).
[20] Roche Diagnostics, ATP Bioluminescence Assay Kit HS II, Instructions for Use, ⟨https://www.sigmaaldrich.com/deepweb/assets/sigmaaldrich/product/documents/342/054/11699709001.pdf⟩, 2021 (accessed 30 January 2026).
[21] Hamidon, N.N., Salentijn, G.I., Verpoorte, E., 2021. Enhanced passive mixing for paper microfluidics. RSC Adv 11 (41), 25677–25685. https://doi.org/10.1039/D1RA04916J.
[22] Mentele, M.M., Cunningham, J., Koehler, K., Volckens, J., Henry, C.S., 2012. Microfluidic paper-based analytical device for particulate metals. Anal Chem 84 (10), 4474–4480. https://doi.org/10.1021/ac300309c.
[23] Chang, C.W., Wang, L.J., 2015. Impact of culture media and sampling methods on Staphylococcus aureus aerosols. Indoor Air 25, 488–498. https://doi.org/10.1111/ina.12162.
[24] Han, Y., Yang, T., Xu, G., Li, L., Liu, J., 2020. Characteristics and interactions of bioaerosol microorganisms from wastewater treatment plants. J Hazard Mater 391, 122256. https://doi.org/10.1016/j.jhazmat.2020.122256.
[25] Kalogerakis, N., Paschali, D., Lekaditis, V., Pantidou, A., Eleftheriadis, K., Lazaridis, M., 2005. Indoor air quality—bioaerosol measurements in domestic and office premises. J Aerosol Sci 36 (5-6), 751–761. https://doi.org/10.1016/j.jaerosci.2005.02.004.
[26] Rangaswamy, B.E., Francis, F., Prakash, K.K., Manjunath, N.S., 2013. Variability in airborne bacterial and fungal population in the tertiary health care centre. Aerobiology 29, 473–479. https://doi.org/10.1007/s10453-013-9297-z.
[27] Currie, L.A., 1968. Limits for qualitative detection and quantitative determination. Application to radiochemistry. Anal Chem 40 (3), 586–593.
[28] Heo, K.J., Ko, H.S., Jeong, S.B., Kim, S.B., Jung, J.H., 2021. Enriched aerosol-to-hydrosol transfer for rapid and continuous monitoring of bioaerosols. Nano Lett 21 (2), 1017–1024. https://doi.org/10.1021/acs.nanolett.0c04096.
[29] Yoon, K.Y., Park, C.W., Byeon, J.H., Hwang, J., 2010. Design and application of an inertial impactor in combination with an ATP bioluminescence detector for in situ rapid estimation of the efficacies of air controlling devices on removal of bioaerosols. Environ Sci Technol 44, 1742–1746. https://doi.org/10.1021/es903437z.
[30] Park, C.W., Park, J.-W., Lee, S.H., Hwang, J., 2014. Real-time monitoring of bioaerosols via cell-lysis by air ion and ATP bioluminescence detection. Biosens Bioelectron 52, 379–383. https://doi.org/10.1016/j.bios.2013.09.015.
[31] Tong, Y., 1999. Diurnal distribution of total and culturable atmospheric bacteria at a rural site. Aerosol Sci Technol 30, 246–254. https://doi.org/10.1080/027868299304822.
[32] Braissant, O., Astasov-Frauenhoffer, M., Waltimo, T., Bonkat, G., 2020. A review of methods to determine viability, vitality, and metabolic rates in microbiology. Front Microbiol 11, 547458. https://doi.org/10.3389/fmicb.2020.547458.
[33] Canyelles i Font, F., Żukowski, K., Khan, M.A., Kwiatek, D., Kolanowski, J.L., 2024. Interference of metal ions on the bioluminescent signal of firefly, Renilla, and NanoLuc luciferases in high-throughput screening assays. Front Chem 12, 1436389. https://doi.org/10.3389/fchem.2024.1436389.
[34] Bowers, R.M., McCubbin, I.B., Hallar, A.G., Fierer, N., 2012. Seasonal variability in airborne bacterial communities at a high-elevation site. Atmos Environ 50, 41–49. https://doi.org/10.1016/j.atmosenv.2012.01.005.
[35] Woo, A.C., Brar, M.S., Chan, Y., Lau, M.C., Leung, F.C., Scott, J.A., et al., 2013. Temporal variation in airborne microbial populations and microbially-derived allergens in a tropical urban landscape. Atmos Environ 74, 291–300. https://doi.org/10.1016/j.atmosenv.2013.03.047.
[36] Ruiz-Gil, T., Acuña, J.J., Fujiyoshi, S., Tanaka, D., Noda, J., Maruyama, F., et al., 2020. Airborne bacterial communities of outdoor environments and their associated influencing factors. Environ Int 145, 106156. https://doi.org/10.1016/j.envint.2020.106156.
[37] Fennelly, M.J., Sewell, G., Prentice, M.B., O'Connor, D.J., Sodeau, J.R., 2017. The use of real-time fluorescence instrumentation to monitor ambient primary biological aerosol particles (PBAP). Atmosphere 9 (1), 1. https://doi.org/10.3390/atmos9010001.
[38] Liu, Q., Yan, S., Zhang, M., Wang, C., Xing, D., 2024. Air sampling and ATP bioluminescence for quantitative detection of airborne microbes. Talanta 274, 126025. https://doi.org/10.1016/j.talanta.2024.126025.